PALEOENVIRONMENTAL CONTROLS ON DIAGENESIS OF ORGANIC-RICH SHALES IN THE EAGLE FORD GROUP

A Thesis

by

KENDRA RAE KRUSE

Submitted to the Office of Graduate and Professional Studies of
Texas A&M University
in partial fulfillment of the requirements for the degree of

MASTER OF SCIENCE

Chair of Committee,	Michael M. Tice
Committee Members,	Michael C. Pope
	Walter B. Ayers
Head of Department,	John R. Giardino

December 2014

Major Subject: Geology

ABSTRACT

Carbonate precipitation can be either promoted or inhibited by microbial processes in different redox zones. It is therefore possible for basin redox evolution to indirectly control early carbonate diagenesis and modify reservoir properties of corresponding shale units. The goals of this study were to analyze geochemical characteristics of the Late Cretaceous Eagle Ford Group in McMullen County, Texas to test the hypotheses that (1) the redox state of the water column controlled carbonate cement abundance and (2) carbonate cement lowered organic matter content by volumetric dilution. An x-ray analytical microscope was used to map elemental compositions of fresh core samples within the Eagle Ford Group. Resultant maps were used to characterize carbonate cements and to estimate the redox state of the overlying water column during deposition, as indicated by the relative abundances of the trace metals Mo, V, and Cr.

Results indicate that cementation occurred early relative to compaction. Ti Kα1 normalized Mo Kα1 and Ca Kα1 fluorescence intensities are positively correlated throughout the unit, suggesting that carbonate cementation was related to the redox state. Total organic carbon is negatively correlated in the upper Lower Eagle Ford with (Ca Kα1)/(Ti Kα1) fluorescence ratio, consistent with volumetric dilution of organic matter by diagenetic cementation prior to compaction. In contrast, there is no significant correlation between total organic carbon and carbonate content in the more organic-rich Lower Eagle Ford.

TABLE OF CONTENTS

Page

ABSTRACT…….…... ii

TABLE OF CONTENTS……. iii

LIST OF FIGURES……. iv

LIST OF TABLES …….. v

1. INTRODUCTION.....1

1.1 Objective 2
1.2 Carbonate Precipitation 2
1.3 Water Column Redox State.....4
1.4 Geologic Background.....7

2. METHODS.....11

2.1 Core Preparation.....11
2.2 XRF Scanning Methods 11
2.3 ImageJ Methods 13

3. RESULTS.....14

3.1 Lithofacies 15
3.2 Burrows 17
3.3 Elemental and Organic Composition 18

4. DISCUSSION 24

4.1 Early Cementation.....24
4.2 Relationship of Carbonate Content and TOC.....25
4.3 Paleoredox Zone Analysis.....26
4.4 Paleoredox Zone in Core.....28
4.5 Relative Importance of Dilution and Paleoredox Controls on TOC, Carbonate, and Metal Abundances 30

CONCLUSIONS.....35

REFERENCES.....36

LIST OF FIGURES

Page

Figure 1. Study area and geographic features in Texas during the Cenomanian - Turonian. 10

Figure 2. Well log showing formation top correlations. 12

Figure 3. Pyrite-filled vein. 15

Figure 4. Massive lithofacies of the Eagle Ford Group. 16

Figure 5. Laminated lithofacies of the Eagle Ford Group. 17

Figure 6. Pyrite-filled burrow from the Eagle Ford Group. 18

Figure 7. All parameters used for redox zone determination. 19

Figure 8. Areas of low Ca/Ti abundance in the Eagle Ford Group. 20

Figure 9. Sample with high Ca/Ti abundance in the Eagle Ford Group. 21

Figure 10. Variations in pyrite grain size in the core. 22

Figure 11. Metal enrichments recording changes in anaerobic conditions. 23

Figure 12. Carbonate nodule that was cemented soon after deposition. 25

Figure 13. Ca/Ti vs. TOC weight percent in the Eagle Ford Group. 26

Figure 14. Redox zone vs. core depth. 29

Figure 15. Location of redox zone influenced by deposition in the Eagle Ford. 31

Figure 16. Ca/Ti and TOC abundance averages per zone. 32

Figure 17. Mo/Ti vs. Ca/Ti fluorescence ratios for the lower and upper lower Eagle Ford. 33

Figure 18. Mo/Ti vs TOC weight percent in the Eagle Ford Group. 34

LIST OF TABLES

Page

Table 1. Bacterial metabolic reactions. 7

Table 2. Redox zone classification chart.....28

Table 3. Averages of abundances of TOC and Ca concentration by redox zone.....32

1. INTRODUCTION

The Cenomanian-Turonian Eagle Ford Group is well known as a hydrocarbon source for carbonate reservoirs in Texas (Fertl and Reike, 1979). Recent developments in production technology have allowed the Eagle Ford Group and other fine-grained petroleum source rocks to be exploited as unconventional hydrocarbon resource plays. Success of individual resource plays, in general, has varied widely (Hildred et al., 2011; Swindell, 2012). This variation may be attributed to paleo-environmental factors controlling the enrichment of organics (Sageman, 2004) based on microbial processes occurring during deposition (i.e. redox state of the overlying water column). More research into redox state controls on organic richness may provide a method to use paleo-environmental proxies to geosteer within a target zone and a better understanding of geological parameters and production outcomes of these resource plays.

Early carbonate cements have the potential to alter rock properties that are important for hydrocarbon production, and carbonate mineral saturation can be alternately decreased or increased by microbial processes restricted to different redox respiration zones (Froelich, 1979; Canfield and Raiswell, 1991; Vissher et al., 2000; Warthmann et al., 2000). Most metabolic processes by micro-organisms create bicarbonate as a product of the reaction. When aerobic metabolic processes are not possible, anaerobic processes will use organic carbon and produce elevated alkalinity which will control the amount of carbonate minerals in the system (Schrag, 2013). It is therefore possible that the redox evolution of the local water column may have indirectly

controlled early diagenesis and modified the reservoir properties of Eagle Ford Group horizons.

1.1 Objective

I tested the model that the redox evolution of the overlying water column controlled or constrained carbonate cementation during early diagenesis of the Eagle Ford Group. Geochemical characteristics of the Late Cretaceous Eagle Ford Group in McMullen County, Texas were analyzed to test the hypotheses that (1) the redox state of the water column controlled carbonate cement abundance, and (2) carbonate cement lowered organic matter content by volumetric dilution. These results may be useful for future studies intended to determine the relative importance of organic matter primary production, preservation during burial, and dilution by cements on total organic carbon (TOC) throughout this part of the Eagle Ford Group. Additionally, these results may have bearing on understanding other carbonate-rich unconventional reservoirs.

1.2 Carbonate Precipitation

Diagenetic carbonate precipitation in modern sediments is promoted by sulfate reduction and other anaerobic metabolic processes (Froelich, 1979; Canfield and Raiswell, 1991; Vissher et al., 2000; Warthmann et al., 2000; Van Lith et al., 2002). These same processes are thought to be the source of concretions and abundant carbonate cements that formed in ancient sediments (Scotchman, 1991). Carbonate

precipitation during sulfate reduction is promoted through the coupling of the following two reactions:

$$SO_4^{2-} + 2CH_2O \rightarrow HS^- + 2HCO_3^- + H^+ \quad (1)$$

$$Ca^{2+} + HCO_3^- \rightarrow CaCO_3 + H^+ \quad (2)$$

In reaction 1, the production of bicarbonate can elevate the saturation index for calcium carbonate which drives precipitation by reaction 2 when hydrogen sulfide is lost from pore fluids (Bosak and Newman, 2003). Alternatively, sulfate-reducing bacteria may serve as nucleation sites for carbonate precipitation (Bosak and Newman, 2003).

Microbial iron reduction (reaction 3) produces an increase of alkalinity that may drive carbonate precipitation in reactive, ferric-iron rich sediments (Froelich, 1979; Coleman, 1985; Zeng and Tice, 2014). In this reaction, seven protons are consumed per bicarbonate ion produced; thus, carbonate cementation has the potential to incorporate significant organic carbon from the water column relative to bicarbonate derived from anaerobic respiration.

$$4FeOOH + CH_2O + 7H^+ \rightarrow 4Fe^{2+} + HCO_3^- + 6H_2O \quad (3)$$

This suite of reactions suggests that microbially promoted carbonate mineral precipitation could contribute significantly to sedimentary carbon budgets. In particular, cementation may become a significant component of long-term basin carbon budgets under circumstances in which Ca^{2+} and HCO_3^- can diffuse readily into sediments during iron and sulfate reduction within anaerobic intervals (Schrag, 2013).

1.3 Water Column Redox State

Trace elements in the water column may be fixed into the sediment if they adsorb to solids or form mineral precipitates. In oxygen-depleted environments, the trace elements (V, Cr, Mn, Co, Ni, Zn, Mo, U) can move from the water column to the sediment through diffusion or remobilization within the sediments along redox gradients (Tribovillard et al., 2006). Mo and V are highly sensitive to changes in redox states (Breit and Wanty, 1991; Wanty and Goldhaber, 1992; Tribovillard et al., 2006); they can be used to indicate the distribution of oxidation states across depositional and diagenetic boundaries (Tribovillard et al., 2006). Both Mo and V have minimal detrital sources, making authigenic processes the dominant sources of these metals in sediments (Tribovillard et al., 2006). Sediments deposited under sulfidic water columns tend to be enriched in these two redox-sensitive elements, making them excellent paleoredox proxies (Tribovillard et al., 2006).

1.3.1 Vanadium

Vanadium is a good indicator of water chemistry, because there are distinct chemical behaviors in each possible oxidation state: (III); (IV); and (V) (Wanty and Goldhaber, 1992). Redox conditions along with adsorption are the main controls on V solubility and biogeochemical cycling. When anoxic conditions persist V(V), vanadate, is reduced to V(IV) (Breit and Wanty, 1991). In euxinic conditions, V(IV) may be further reduced to V(III) by H_2S. H_2S helps organic matter accumulation because it keeps competing ions, such as Ni, from binding and using the organic complexes. Two

possible thermodynamic reactions for reducing V(IV) to V(III) were studied by Wanty and Goldhaber (1992) and reported as follows:

$$VO(OH)^{+} + 0.5H_2S \leftrightarrow V(OH)_2^{+} + 0.5S^0 \quad (4)$$

$$VO(OH)^{+} + 0.5HS^{-} + 0.5H^{+} \leftrightarrow V(OH)_2^{+} + 0.5S^0 \quad (5)$$

Vanadium in both reduced states, V(IV) and V(III), can be adsorbed onto particulate organic matter (Bellanca et al., 1996). V(III) can also precipitate as the hydroxide $V(OH)_3$ or solid oxide V_2O_3 phase and may be adsorbed to geoporphyrins (Tribovillard et al., 2006). V(III) substitutes for Al in diagenetic environments in both authigenic and recrystallizing clay minerals (Breit and Wanty, 1991; Tribovillard et al., 2006).

Vanadium is most commonly accumulated due to the preservation/increased influx of organic matter during deposition (Breit and Wanty, 1991), through sulfate reduction. If the chemical composition of the water column remains anoxic during post depositional sedimentation, vanadium will be immobile, and therefore it will be preserved efficiently during early diagenesis (Bellanca et al., 1996). Since the sediments are reducing when microbial sulfate reduction is occurring, it is easier for vanadium and other metals to be effectively preserved in the sediments (Bellanca et al., 1996).

1.3.2 Molybdenum

Mo is more enriched than any other metal in anoxic deposits (Calvert and Pedersen, 1993). Input of Mo into waters is normally in the soluble form, molybdate, which remains in solution, unless H_2S concentrations are elevated (Tissot et al., 2012).

Elevated Mo abundances are thus key indicators of sulfidic conditions (Sageman, 2004; Tribovillard, 2006).

Euxinic sediments strongly correlate with high concentration of Mo and TOC in modern and Phanerozoic deposits (Tissot et al., 2012). Sulfidic environments enrich deposits in Mo by converting molybdate (MoO_4^{2-}) to oxythiomolybdates ($MoO_xS_{4-x}^{2-}$), a form that can more readily be incorporated in sediments (Tissot et al., 2012). Eventually, the oxythiomolybdates will be converted into a reactive thiomolybdate (MoS_4^{2-}). The complete reaction is as follows:

$$MoO_4^{2-} + 4H_2S_{(aq)} \leftrightarrow MoS_4^{2-} + 4H_2O \qquad (6)$$

1.3.3 Redox State Classification

Geochemical environments commonly are classified as either oxic or disoxic. However, within anoxic environments there are a series of distinct redox zones controlled by different microbial respirations (Froelich, 1979, Tribovillard, 2006, Canfield and Thamdrup, 2009). When oxygen is depleted, denitrification, manganese reduction, iron reduction, and sulfate reduction will begin in sequential order. For this study, the anaerobic zone will be analyzed in terms of the redox zone (bacterial respiration) present during deposition (Table 1).

Bacterial Metabolic Reactions

Oxic Respiration (Aerobic)
$CH_2O + O_2 \rightarrow HCO_3^- + H^+$
Denitrification
$CH_2O + 2NO_3\text{-} \rightarrow HCO_3^- + H^+ + 2NO_2^-$
Mn Reduction
$CH_2O + 2MnO_2 + 3H^+ \rightarrow HCO_3^- + 2Mn^{2+} + 2H_2O$
Fe Reduction
$CH_2O + 7H+ + 4Fe(OH_3) \rightarrow HCO_3^- + 4Fe^{2+} + 10H_2O$
Sulfate Reduction
$SO_4^{2-} + 2CH_2O \rightarrow 2HCO_3^- + HS^- + H^+$

Table 1. Bacterial metabolic reactions. Each represents a distinct redox zone. Since they were not distinguishable by proxies used in this study, denitrification and Mn reduction are combined for paleoenvironmental interpretations.

1.4 Geologic Background

The Cenomanian-Turonian Eagle Ford Group is composed of organic-rich limestone, argillaceous limestone, and calcareous mudstone that were deposited throughout parts of Texas and northwestern Mexico (Dawson and Almon, 2010; Hentz and Ruppel, 2010; Driskell et al., 2012; Quirein et al., 2012). The 92 Ma Cenomanian-Turonian boundary occurs within the Eagle Ford Group and was identified as a major condensed interval that can be correlated globally (Dawson and Almon, 2010). This condensed interval marks a maximum flooding surface formed during the highest eustatic sea level rise in the Phanerozoic (Driskell et al., 2012). At this high eustatic sea

level, abundant source rock, coeval to the Eagle Ford Group, was deposited throughout the United States and other parts of the world. Deep marine suboxic zones expanded during the Cretaceous in a series of oceanic anoxic events (OAEs), possibly because of poor ocean mixing resulting from shallow latitudinal thermal gradients (Arthur and Schlanger, 1979). This lack of oxygen promoted the preservation of organic material in many areas (Driskell et al., 2012).

When the Eagle Ford Group was deposited, the Western Interior Seaway, an epeiric sea, occupied much of current-day west Texas. When isolated bodies of water, like those within the Western Interior Seaway, undergo extensive organic matter input, a chemically stratified water column may be produced (Jenkyns, 2010). These conditions make possible a geochemical change from poorly oxygenated to anoxic and ultimately euxinic conditions to occur (Jenkyns, 2010) throughout the water column.

The Eagle Ford Group was subdivided into two informal members based on gamma ray, SP, and resistivity log characteristics (Adams and Carr, 2010; Driskell, 2012). This division can be correlated regionally across the 19,500 mi^2 Eagle Ford play (Quirein, 2012). Regional correlation demonstrates lateral and vertical variations within the Eagle Ford Group. In the southwest it ranges from approximately 300 to 660 feet thick at a depth of 14,000 to 15,600 feet (Hentz and Ruppel, 2010; Quirein, 2012; Tian et al., 2012). The Eagle Ford thins northeastward to approximately 50 feet thick at a depth of 4,000 feet as it approaches the San Marcos Arch (Quirein, 2012; Tian et al., 2012).

The 65-meter (214-ft) Eagle Ford Group core analyzed in this study is from McMullen County in the Rio Grande Embayment (Figure 1). The Eagle Ford Group in this area is predominantly calcareous mudstone. The organic-rich shales of the Eagle Ford were deposited in an oxygen deficient to anoxic marine environment (Charvat and Grayson, 1981; Dawson, 2006). The Eagle Ford Group's dark color, millimeter-scale laminae, authigenic pyrite, high ratio of pelagic to benthic fossils, and lack of infauna were interpreted as environmental indicators of anoxia (Charvat and Grayson, 1981) that locally prevailed during the global highstand. In this specific core, much of the typical Upper Eagle Ford was either eroded or not deposited. For this study, samples were only taken from the Lower Eagle Ford, which is informally divided into the upper Lower Eagle Ford and the lower Lower Eagle Ford based on geochemical properties.

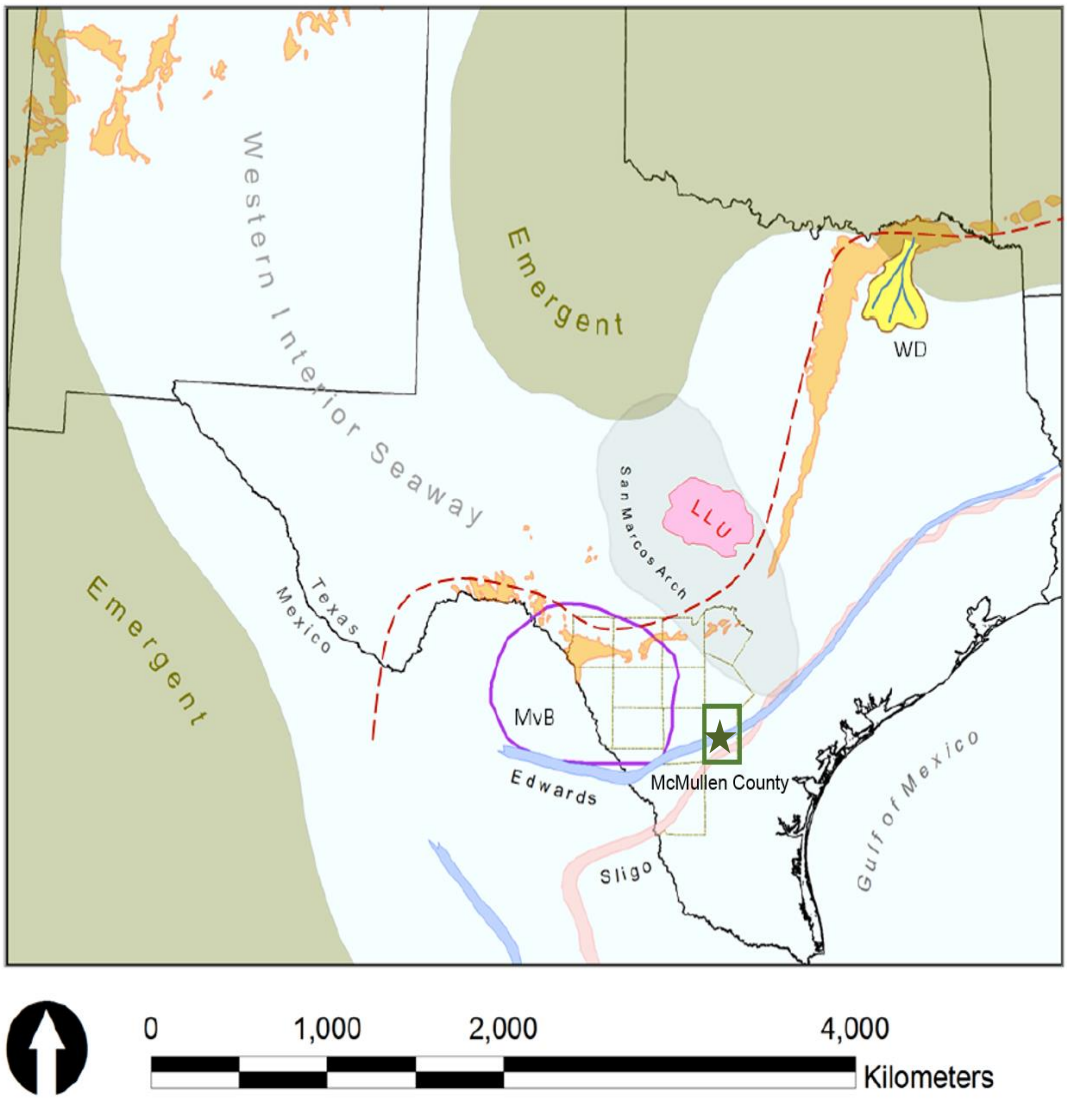

Figure 1. Study area and geographic features in Texas during the Cenomanian - Turonian. Study area, McMullen County is highlighted with a green outline and a green star representing the approximate well location. Features include Western Interior Seaway, Cretaceous shelf edges [Sligo (pink ribbon) and Edwards (blue ribbon)], Maverick Basin (MvB – purple outline), Woodbine Delta (WD), San Marcos Arch (grey oval), Llano Uplift (LLU – pink polygon), and the Quachita Mountain front (red dash line). Eagle Ford Group outcrops are colored orange. All counties identified represent Rio Grande Embayment where the study area is located. *Modified from Driskell et al., 2012*.

2. METHODS

2.1 Core Preparation

Three-inch core was obtained from Murphy Exploration and divided into 33 distinct hand samples for facies analysis (Figure 2). Each hand sample is approximately 3 in. long, with two of the hand samples being 2 ft long. Murphy Exploration also provided gamma ray, SP, resistivity, neutron and density porosity well logs for the cored interval. The logs were run and calibrated by Baker Hughes. The core samples were sent to Weatherford Labs for total organic carbon analysis, which was determined by Rock Eval pyrolysis.

2.2 XRF Scanning Methods

Fresh samples from the Eagle Ford Group core were scanned by x-ray fluorescence (XRF) microscopy (Horiba XGT-7000 X-Ray Analytical Microscope) to gather elemental distribution data. Scans were conducted at 100 μm resolution to yield element maps representing the distribution for the sample. A fluorescence peak analysis was conducted to determine the elements in each core section.

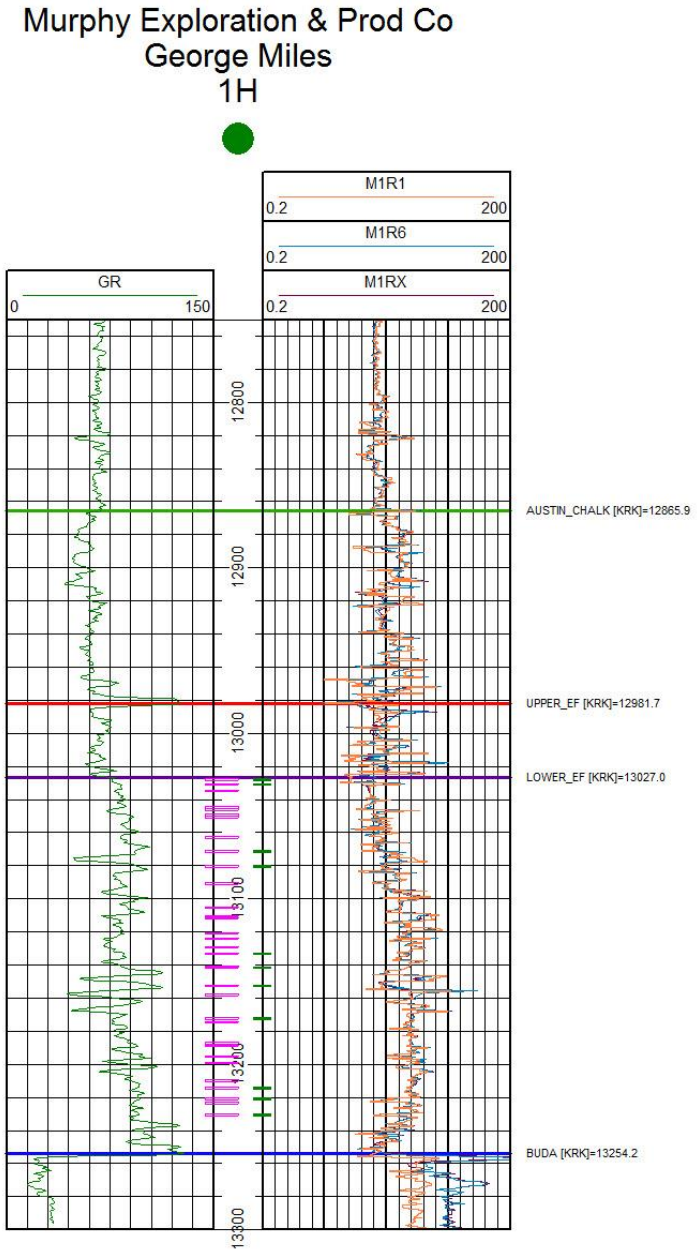

Figure 2. Well log showing formation top correlations. The pink markers indicate samples taken. Green markers indicate figure locations in this report.

Background noise maps of selected elements were calculated and subtracted from appropriate element maps. Resultant maps were used to estimate the redox state of the overlying water column during deposition, using the presence or absence of iron-lined laminae, presence of burrows, and the abundances of redox-sensitive elements such as Mo, V, Cr, and Zn. These data were analyzed by a Java-based image processing program, ImageJ.

2.3 ImageJ Methods

Elemental maps were uploaded and background noise was subtracted for Ca, S, Fe, Mo, Ti, Zn, V, and Cr to generate gray-scale images. The resulting images were analyzed using a number of techniques to extract relevant data including fluorescence intensity values. A Fast Fourier Transform (FFT) was performed on Fe images for identification of laminae. Composite color images of Ca, Fe and S were made to determine the distributions of pyrite and carbonate cements.

3. RESULTS

Fluorescence intensities for redox-sensitive elements and Ca were normalized to Ti fluorescence intensity to correct for variations in sample distance to the x-ray collector or x-ray source output. Titanium has the same wave length characteristics as many of the targeted elements based on molecular weight, making it the best candidate for normalization. This normalization accounted for variations in instrument x-ray output or distance to the sample.

X-ray images that were created using the analytical microscope also were used in all analysis. This allowed characterization of the core not only based on what is on the surface, but also what is present within the rock. The x-ray images allowed identification of burrows, carbonate nodules, and pyrite. When analyzing the x-ray images, there were several dark, cube-shaped structures (Figure 3). Based on the cubic shape, nature of distribution, the gold color on the core surface and the increase in Fe and S where located, I inferred these are pyrite crystals.

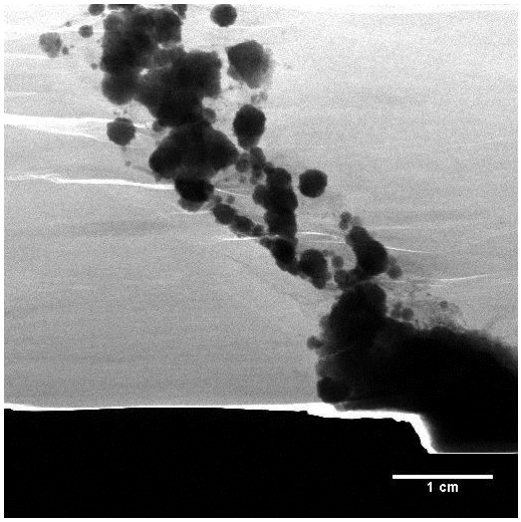

Figure 3. Pyrite-filled vein. X-ray image from depth 13230.1 ft.

3.1 Lithofacies

Two lithofacies, based on physical features, were identified in the Eagle Ford Group. The most abundant lithofacies is massive mudrock (Figure 4). The massive nature of this lithofacies could be caused by extended times of undisturbed deposition or a large amount of bioturbation. Since there is a lack of trace fossils, it is concluded it was caused by undisturbed deposition of similar elemental content.

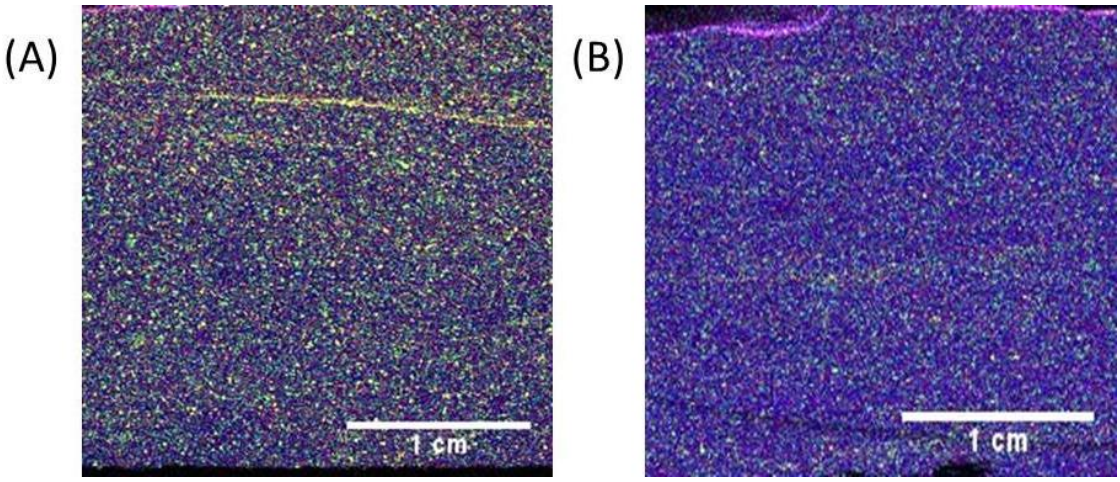

Figure 4. Massive lithofacies of the Eagle Ford Group. Composite images were created by stacking and applying color identifiers to Ca (blue), Fe (red), and S (green). The yellow color indicates pyrite grains. (A) is at depth 13171.8 ft and (B) is at depth 13071.0 ft.

The second lithofacies is a laminated mudrock (Figure 5). The laminations are thin 0.1 cm average thickness and make up laminae sets in most areas of the core. The laminations are well-defined and well-preserved, indicating few to no burrowing organisms were living during deposition, suggesting low oxygen conditions. The composition of the laminations in this lithofacies also were characterized to provide insights into not only sediment depositional conditions but water column chemistry.

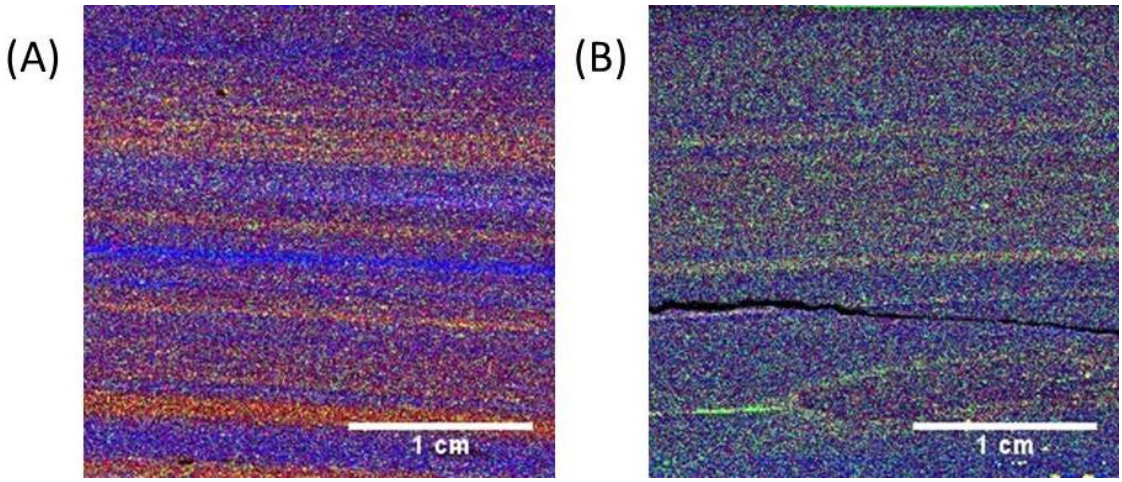

Figure 5. Laminated lithofacies of the Eagle Ford Group. The different colors are caused by different elements making up any particular lamination. When the lamination is blue, there is more Ca present. When the laminations range from red to yellow there are different abundances of Fe and S present. Color scheme is the same as in Figure 3.

3.2 Burrows

Burrows are rare, occurring as pyrite-filled tubes in two of the thirty-seven samples examined. The diameter of the tubes is ~ 2.2 mm when oriented in the vertical direction and ~ 1.4 mm when oriented in the horizontal direction. Orientation is mostly horizontal with rare occasional vertical excursions. The x-ray image shows evidence that there is more horizontal disruption than seen on the surface (Figure 6). Since most of the burrowing is isolated to the horizontal direction and above the main vertical tube, it is thought these could be feeding tubes where the organism was looking for nutrients.

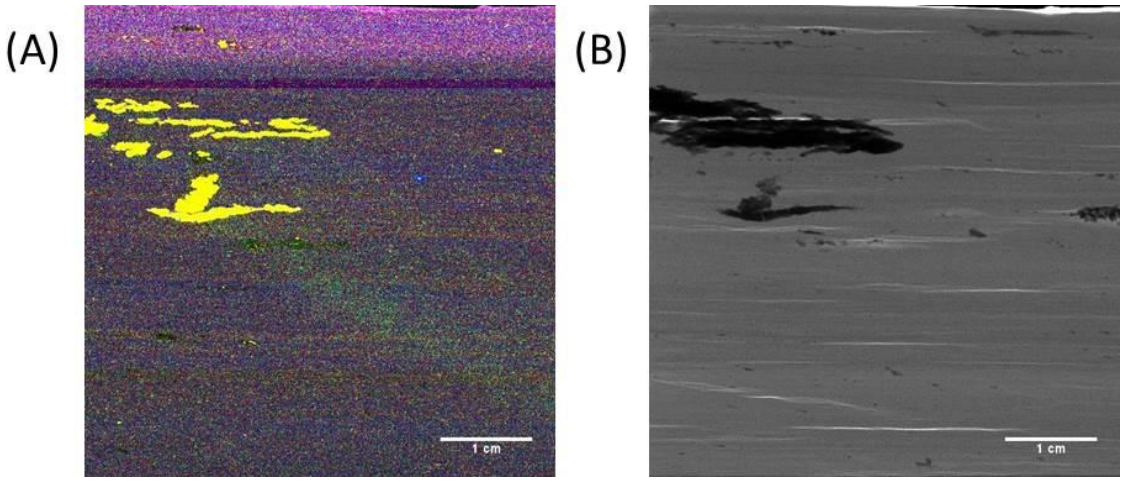

Figure 6. Pyrite-filled burrow from the Eagle Ford Group. (A) Composite image showing pyrite-filled burrow at depth 13,027.5 ft. Color scheme is the same as in Figure 4 (B) X-ray image showing extent of the burrow.

3.3 Elemental and Organic Composition

From the 244 ft. core, thirty-three samples were analyzed for TOC. Total organic carbon (TOC) ranged from 1.7 – 6.3 wt%. Rocks below 13153 ft are more organic-rich than those above (4.62 ± 0.26 wt% vs. 3.5 ± 0.23 wt.%, P=0.003 for a t-test; averages are reported plus or minus one standard error). Based on this distinction the lower Eagle Ford was broken up into two sub-units, the upper lower Eagle Ford which is from the top of the lower Eagle Ford to a depth of 13153 ft, and the lower Eagle Ford being from 13153 ft to the top of the Buda formation.

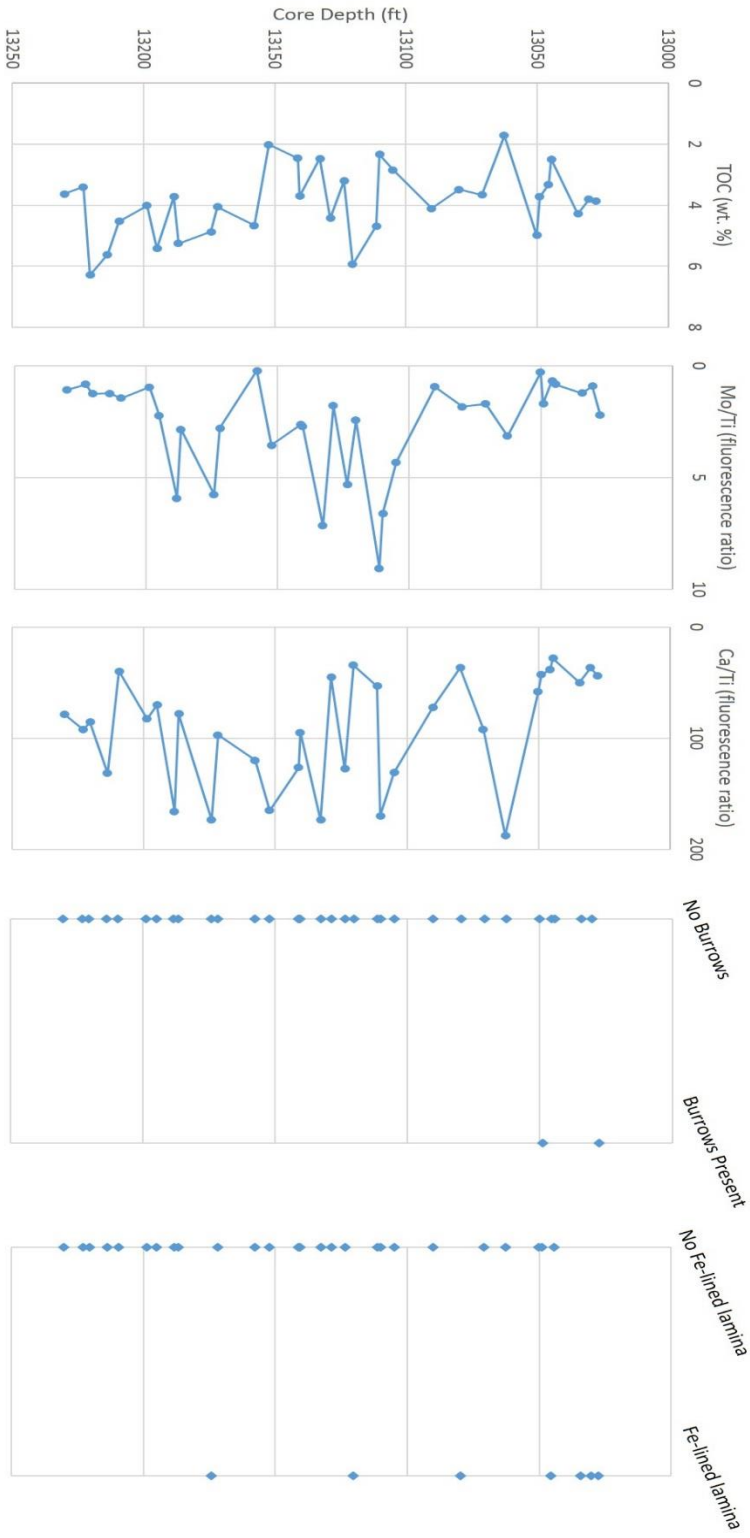

Figure 7. All parameters used for redox zone determination.

3.3.1 Distribution of Calcium

The sample coloring from composite images was used as an initial indication of Ca/Ti abundance but all classification was done using calculated values. Ca Kα1/Ti Kα1 fluorescence ratio ranges from 28-188 (Figure 7). Low calcium concentrations correlate with the laminated mudrock lithofacies. The upper 20 ft of the core has the lowest calcium fluorescence ratio, which correlates to laminations that vary in composition (Figure 8) between pyrite/iron laminations to calcium/sulfur laminations. Other laminations, below 13,050 ft, that have low calcium values are also characterized as laminated mudrock lithofacies.

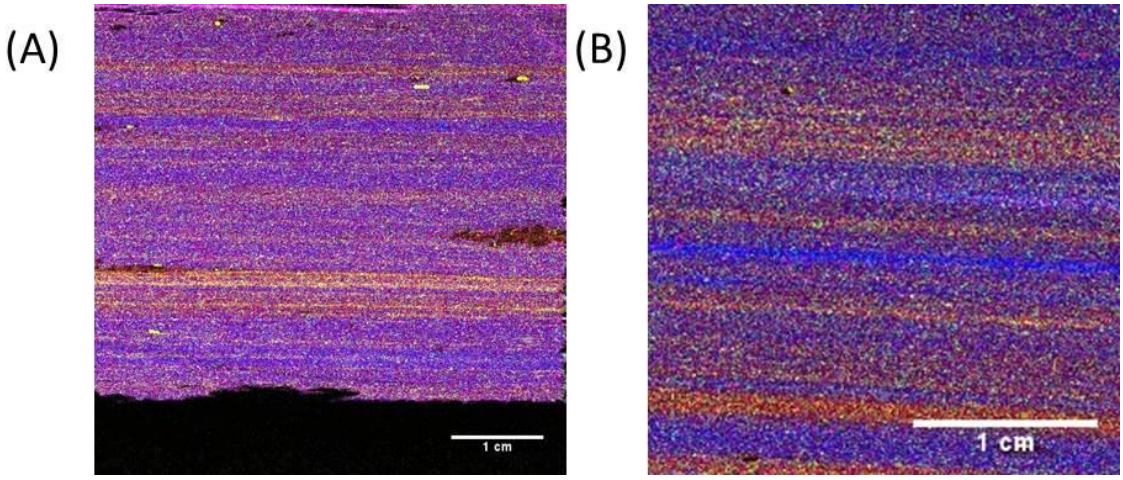

Figure 8. Areas of low Ca/Ti abundance in the Eagle Ford Group. These areas can be initially identified by the overall red and yellow color of the composite image. Since there is low Ca, we do not see much of the blue colored grains. (A) Composite image at depth 13,030.3 ft with a Ca/Ti ratio of 36.82. (B) Composite image at depth 13,079.8 ft with a Ca/Ti ratio of 36.70. Composite images have the same color scheme as Figure 3.

Zones within the core that have high Ca content tend to be the massive mudrock lithofacies. The high Ca content makes the composite image color overall blue (Figure 9). The samples that have high Ca peaks also have significant amounts of yellow grains, pyrite, which are discussed with iron distribution.

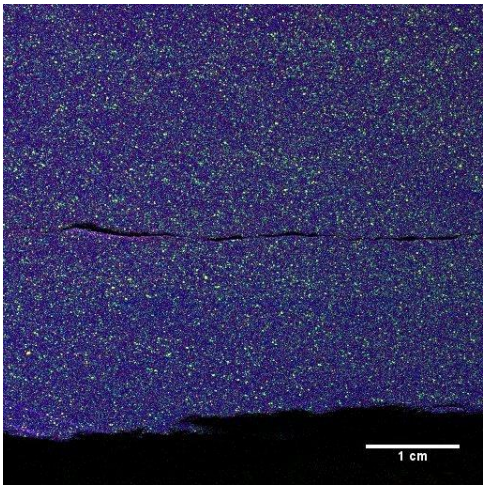

Figure 9. Sample with high Ca/Ti abundance in the Eagle Ford Group. Visually the high Ca abundance can be identified by the overall blue color of the sample. The actual values calculated, 165.21 fluoresence, were used to classify this sample at 13,152.2 ft as having a high Ca/Ti abundance. It was also classified as being the massive lithofacies. This composite image has the same color scheme as Figure 3.

3.3.2 Distribution of Iron

Throughout the core iron occurs in three forms, Fe-lined laminations, pyritic laminations, and as pyrite grains. Pyrite grains vary in size (0.02 - 0.37 cm), and mostly appear in the massive rock lithofacies (Figure 10). In laminations, iron is most likely present in the form of pyrite and, as discussed in the lithofacies section, occur mostly in the upper portion of the core and are rare below 13,050 ft.

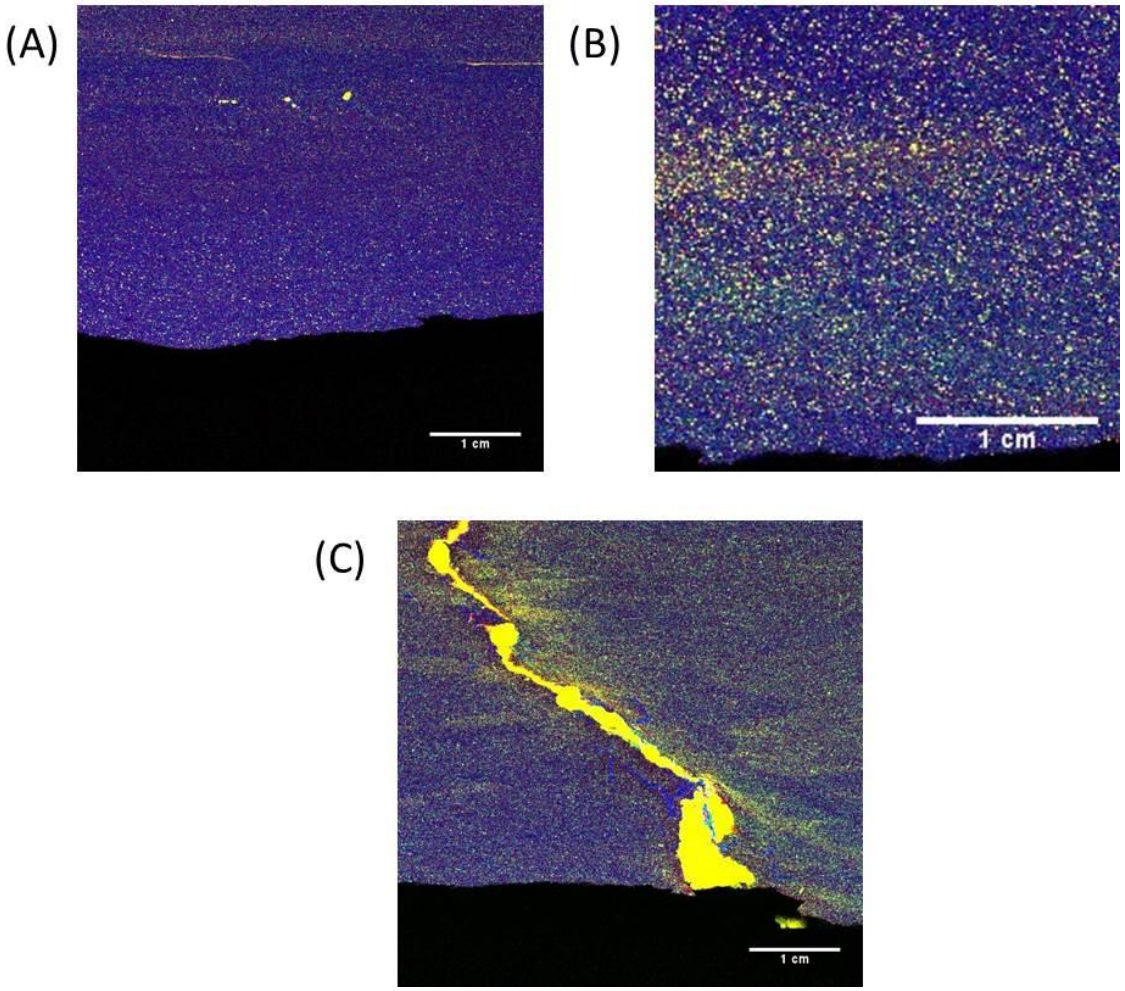

Figure 10. Variations in pyrite grain size in the core. In image A the bigger pyrite grains are 0.05 – 0.1 cm. Image B has grains of 0.025 cm and image C has framboids up to 0.37 cm. The depths for (A), (B), and (C) are 13,141.2 ft., 13,132.8 ft., and 13,230.1 ft. respectfully. These composite images have the same color scheme as Figure 3.

3.3.3 Distribution of Trace Metals (Mo, Cr, V)

Mo/Ti fluorescence ratio ranges from 0.83 to 9.06 (Figure 7). The greatest ratios are in the lower to middle part of the core, and the lowest ratios are at the top and base of

the core. The intervals of elevated Mo fluorescence indicate periods of sulfidic water column conditions.

V/Ti and Cr/Ti fluorescence ratio share the same relationships (increases and decreases) with values ranging from 0.39 to 0.51 and 0.32 to 0.59 respectively (Figure 11). Both of these elements record changes in anaerobic conditions (Tribovillard, 2006), allowing us to see changes in metabolic zonations.

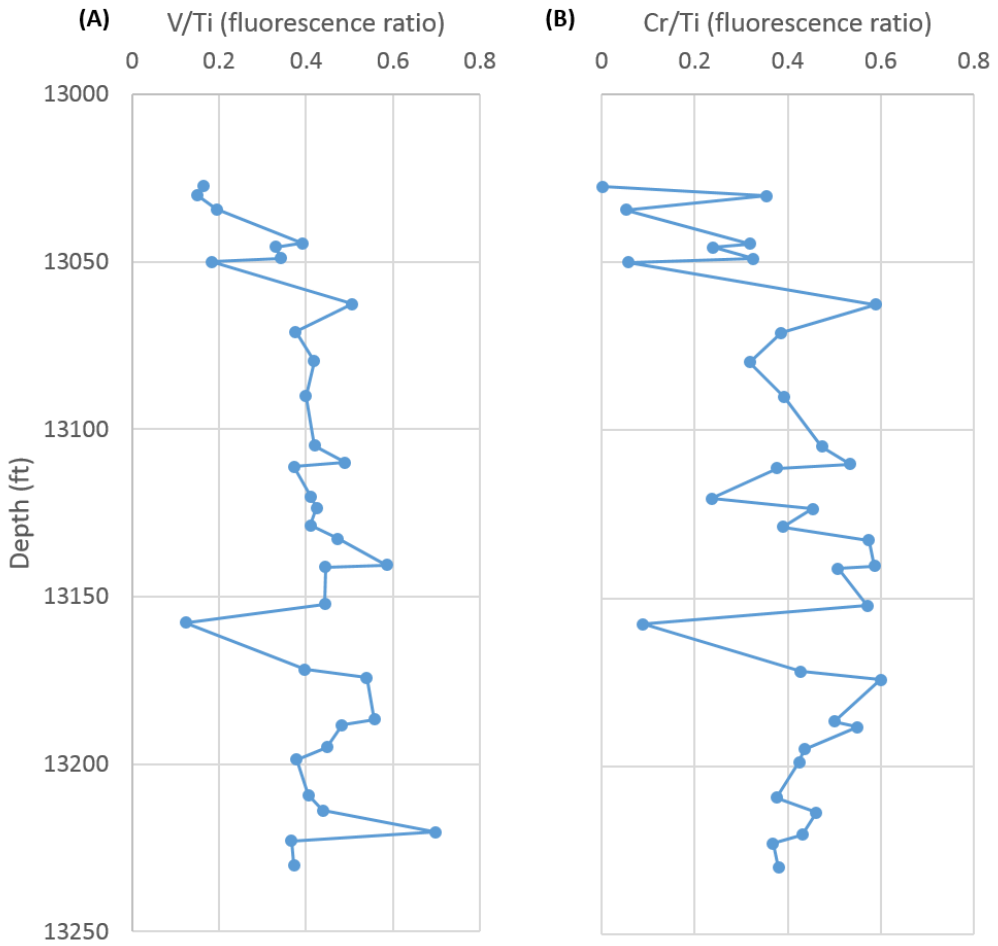

Figure 11. Metal enrichments recording changes in anaerobic conditions.

4. DISCUSSION

4.1 Early Cementation

Throughout the core there is abundant evidence for minimal compaction and localized early cementation. Minimal compaction in the upper portion of the core is well shown at 13,027.5 ft (Figure 6). The burrow here has been compacted by a factor of 1.6, meaning that the diameters of vertical traces are 1.6 times the apparent (compacted) diameters of the same traces in horizontal section. Also, there is little to no deformation in the surrounding rock. The laminations cut by the burrow are not deformed by differential compaction, suggesting that cementation of the entire rock, not pyritization of the burrow, halted compaction.

In the lower portion of the core, there is evidence for local early cementation (Figure 12). The laminations, most evident in the bright yellow (pyritic) lamination just above the nodule, are deformed around it due to differential compaction. This indicates that the nodule was formed early after deposition. Therefore, at least partial carbonate cementation likely occurred during pre-compaction diagenesis.

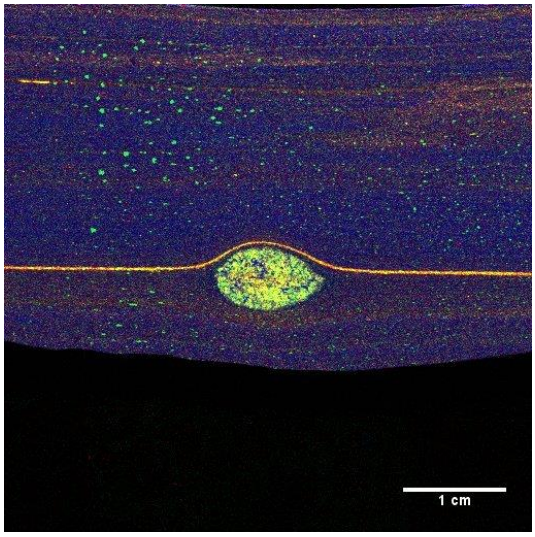

Figure 12. Carbonate nodule that was cemented soon after deposition (depth 13,213.8 ft.) The bright yellow (pyrite replaced) lamination and surrounding beds form around the nodule indicating the formation of the nodule occurred early. This composite image has the same color scheme as Figure 3.

4.2 Relationship of Carbonate Content and TOC

The upper unit of the lower Eagle Ford (Figure 13) has a strong inverse relationship between Ca/Ti ratio and TOC (P = 0.0002 for a t-test on the regression coefficient), suggesting that dilution played a key role in determining final organic content of these rocks. Dilution of organic matter is possible only if cementation occurs early, before the rock is completely compacted, supporting textural interpretations of early cementation. In the lower unit of the Eagle Ford, TOC and Ca/Ti fluorescence ratio do not correlate (P = 0.86 for a t-test on the regression coefficient). Since a different relationship between carbonate content and TOC is apparent in the lower unit, something other than dilution controlled the organic matter content.

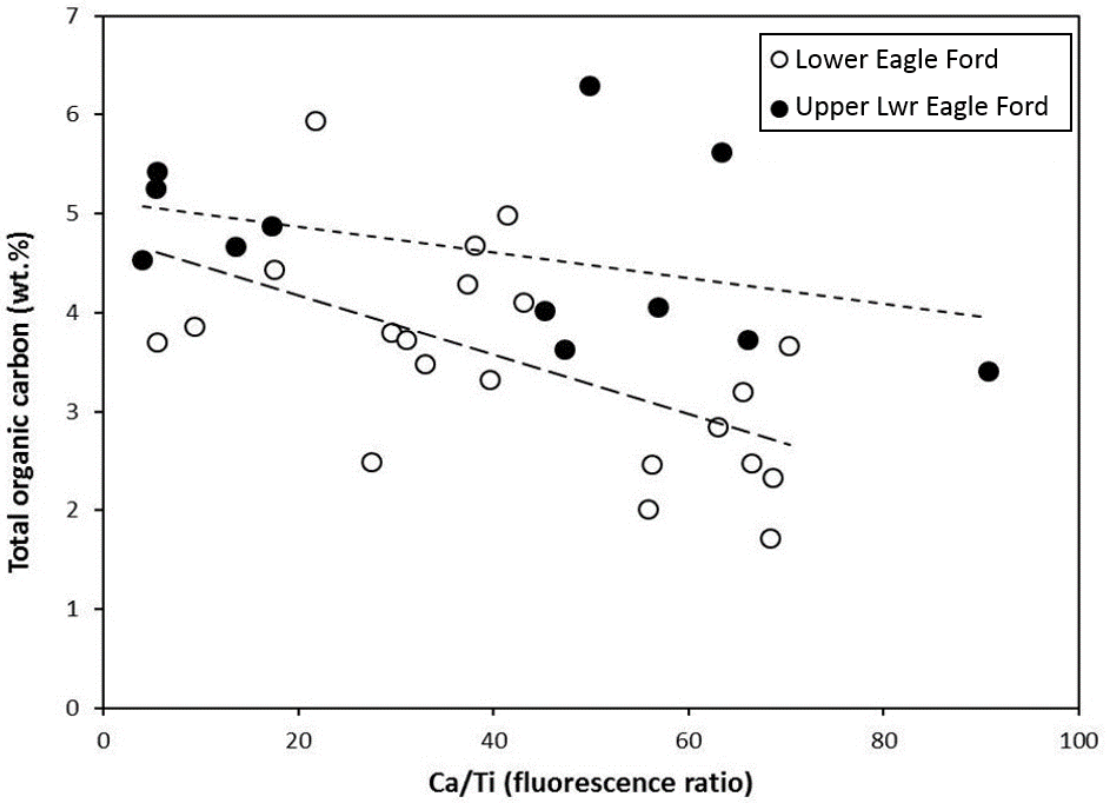

Figure 13. Ca/Ti vs. TOC weight percent in the Eagle Ford Group. Two trend lines are shown, one for the Upper Eagle Ford (long dashed line) and one for the Lower Eagle Ford (short dashed line). The trend lines suggest two possible separate controls on organic matter preservation.

4.3 Paleoredox Zone Analysis

Geochemical and ichnological data were used to analyze the redox state of the water column during deposition of each sample (Table 2). Depending on the redox state, micro-organisms use different electron acceptors for metabolic respiration. Using the classification of different metabolic respirations and their corresponding redox state zones suggested by Canfield and Thamdrup (2009), I determined the four redox state

zones that would be used in this study. When oxygen was present, bioturbation may have occurred, producing rocks with burrows, disrupted laminations, or no preserved sedimentary structures. In zones where manganese or nitrogen was respired, iron would have been oxidized and insoluble in the water column, causing it to be deposited and sorted along with other detrital sediment. The result would have been Fe-lined laminations or other sedimentary structures. In iron reducing zones, iron would have been reduced and soluble, causing it to be incorporated into the sediment in diagenetic precipitates; thus, no Fe-lined laminations would have been formed or preserved.

No elemental concentrations were calculated for this project, and metal accumulation is considered in a relative sense. In order to make a determination of high vs. low metal abundance, a cut-off of 2.5 was used for Mo/Ti fluorescence ratios, because it was consistent with the presence of Fe-lined laminations. All Fe-lined laminations occurred in rocks with Mo/Ti ratios <2.5 and no rocks with ratios >2.5 had Fe-lined laminations.

Based on these distinctions and cutoffs, aerobic conditions were inferred for samples that contained burrows and had low Mo/Ti and V/Ti fluorescence ratios. No distinction was made between the nitrogenous and manganous zones that were inferred for samples that had little to no evidence of bioturbation, presence of Fe-lined laminations, high V/Ti ratios and low Mo/Ti ratios. The ferruginous zone was inferred for samples lacking burrows, bioturbation, and Fe-lined laminations, having high V/Ti ratios, and having low Mo/Ti ratios. The main parameter used to determine the sulfidic zone was a high Mo/Ti ratio, since it is the only redox condition that produces large

accumulations of Mo in sediments (Tribovillard, 2006). The absence of Fe-lined laminations and burrows, in conjunction with a high V/Ti ratio were other parameters used to identify this redox zone.

Redox Zone		**Parameters**
Aerobic		• Bioturbation • No Fe-lined laminations • Low Mo/Ti • Low V/Ti
Anaerobic	Nitrogenous / Manganous	• Fe-lined laminations • High V/Ti • Low Mo/Ti • Little to no bioturbation
	Ferruginous	• No Fe-lined laminations • High V/Ti • Low Mo/Ti • No bioturbation
	Sulfidic	• High Mo/Ti • High V/Ti • No Fe-lined laminations • No bioturbation

Table 2. Redox zone classification chart. Parameters are listed from most indicative to least important.

4.4 Paleoredox Zone in Core

Paleoredox zones were inferred for all samples. 9 of 14 redox transitions between neighboring samples are between paleoredox zones with similar reduction

potentials (i.e., aerobic ↔ nitrogenous/manganous ↔ ferruginous ↔ sulfidic; Figure 14). It is rare to see a thermodynamically predictable transition with a missing redox zone which could simply be the result of the missing zone not being sampled. This profile supports the choice of the cut-offs and redox parameters used in this study.

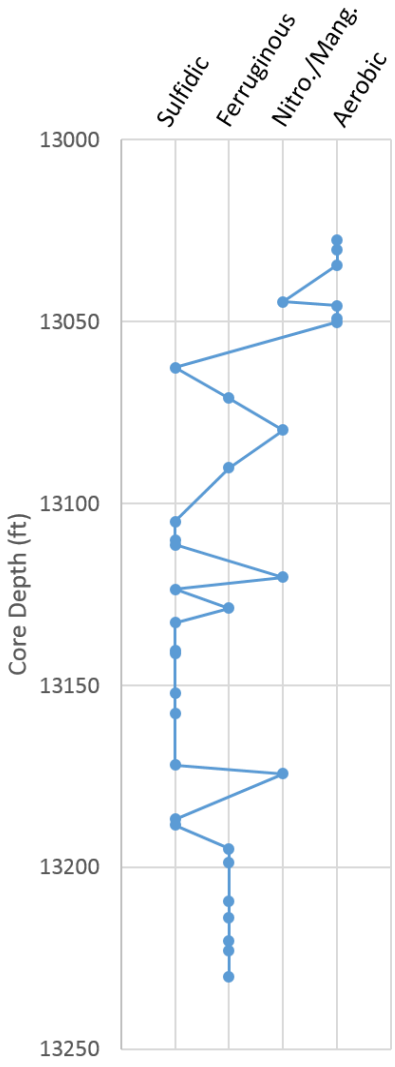

Figure 14. Redox zone vs. core depth. The transition in redox zone demonstrates the change in micro-organisms metabolisms based on available nutrients.

4.5 Relative Importance of Dilution and Paleoredox Controls on TOC, Carbonate, and Metal Abundances

To test the hypothesis that the overlying water column controlled the timing of carbonate cementation and therefore the abundance of carbonate cements, two models for cementation during sulfidic conditions were considered. In the first model, variations in Mo/Ti during euxinia reflect varying intensities of sulfidic conditions in the overlying water column, and more intensely sulfidic conditions promoted earlier carbonate cementation (Figure 15). In this model, weakly sulfidic conditions result in low Ca/Ti and Mo/Ti ratios, whereas strongly sulfidic conditions result in high Ca/Ti and Mo/Ti ratios. There is no reason to expect TOC values to change from the oxic to sulfidic zones, since each type of bacterial respiration (see Table 1), requires the consumption of organic matter. In the second model, variations in Mo/Ti during euxinia reflect varying degrees of incorporation of Mo into the sediment due to varying rates of burial by siliciclastic sediment under relatively constant sulfidic conditions. Slow sedimentation rates would result in intense cementation reflected in high Ca/Ti, minimal dilution of organic input reflected in high TOC, and increased accumulation of Mo. Rapid sedimentation rates would produce low Ca/Ti, TOC, and Mo/Ti.

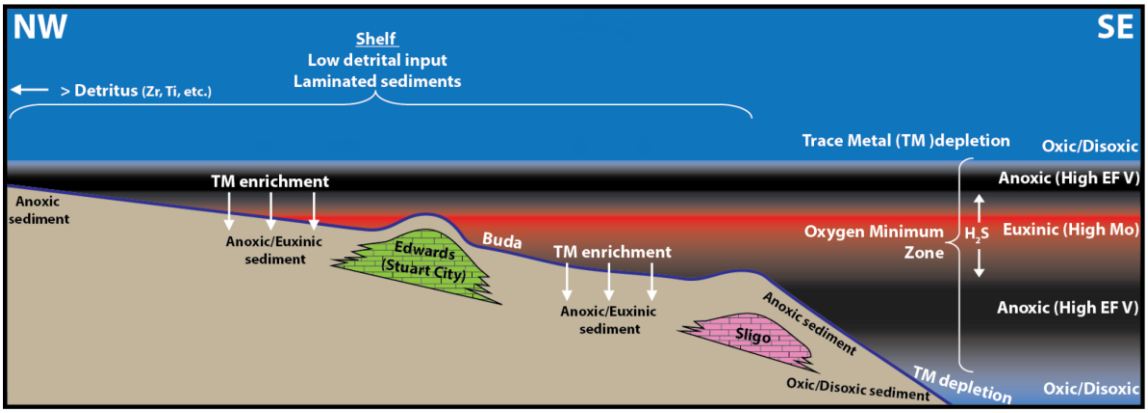

Figure 15. Location of redox zone influenced by deposition in the Eagle Ford**.** *Modified from Tinnin et al, 2013.*

An analysis was done over the entire Eagle Ford Group by redox zone to test the models. Averages of Ca abundance and TOC within each zone support the first model, that carbonate cementation was controlled by variations in euxinia (Table 3; Figure 16). A t-test for two-samples with assumed unequal variances was applied to test the statistical relationship between the aerobic and each anaerobic zones. A Sidak correction was applied with a value of $\alpha_{SID} = 0.0085$, meaning that the critical P value for rejection of the null hypothesis was 0.0085. Rocks from both the ferruginous and sulfidic zones had Ca/Ti ratios significantly greater than rocks of the aerobic zone (P = 0.0011 and 0.0001, respectively). This suggests that there was an increase in carbonate cementation beginning with the ferruginous zone and continuing into the sulfidic zone.

	TOC (wt%)	Ca/Ti fluorescence ratio	Number of Samples
Aerobic	3.993 ± 0.234	45.10 ± 3.263	6
N/Mn	4.195 ± 0.760	68.26 ± 35.14	4
Fe	4.509 ± 0.305	79.13 ± 8.153	10
S	3.202 ± 0.317	130.9 ± 12.37	13

Table 3. Averages of abundances of TOC and Ca concentration by redox zone.

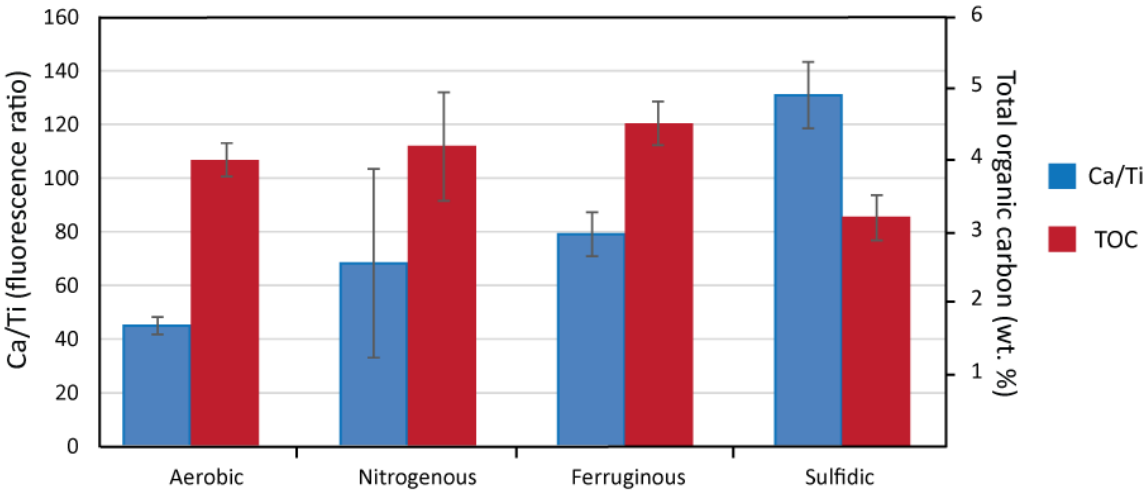

Figure 16. Ca/Ti and TOC abundance averages per zone.

Throughout the core Ca/Ti and Mo/Ti fluorescence ratios are strongly and positively correlated (Figure 17). This relationship indicates that the abundance of carbonate incorporated into the sediment was controlled by the redox state of the overlying water column. A single point on the graph (Mo/Ti = 9.06) does not fall close to the trend line. One possible reason for this could be that diffusive supply of dissolved

Ca to the sediment was cut off for a brief period of time due to rapid burial rates. Mo may have been accumulated since it is controlled by the presence of sulfide in the water column rather than what happens within the sediment. This point is classified as being in the nitrogenous zone and is responsible for the greater value in standard error as seen in Figure 14.

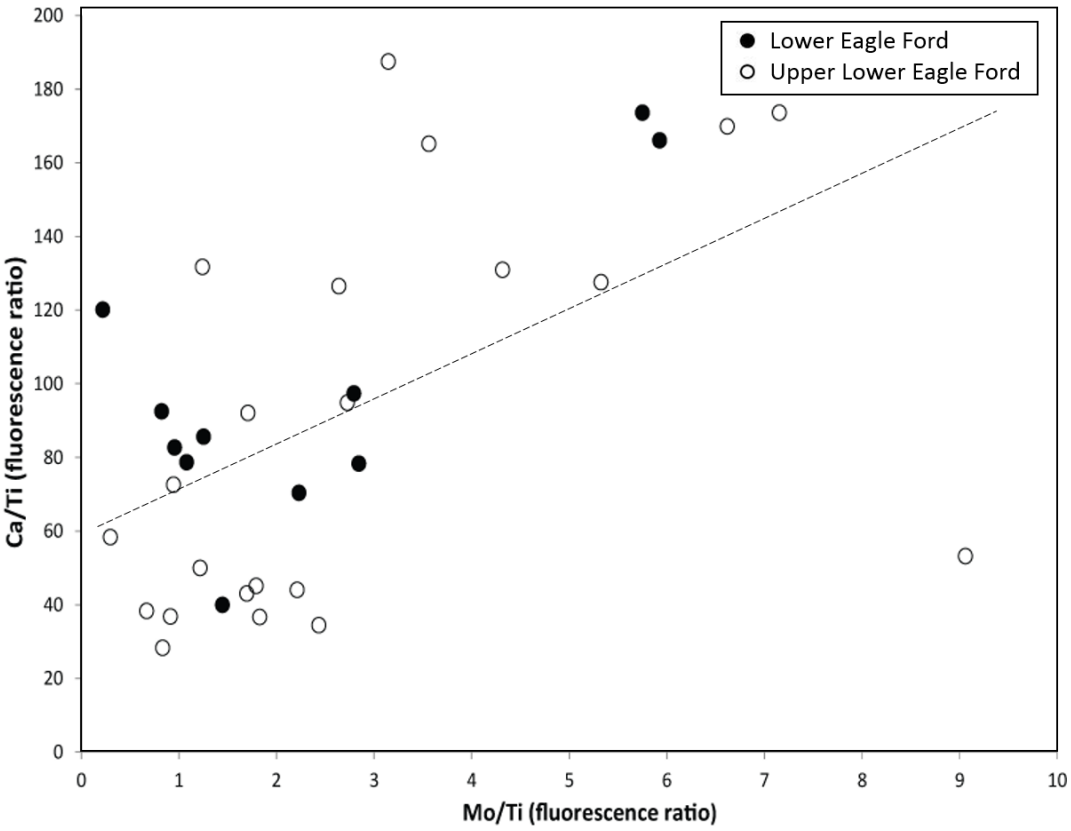

Figure 17. Mo/Ti vs. Ca/Ti fluorescence ratios for the lower and upper lower Eagle Ford. The proximity of both units to the trend line indicates that there is no statistical difference in depositional redox conditions.

There is no relationship (P=0.18) between Mo/Ti fluorescence ratio and TOC (Figure 18) in this core. This indicates that Mo, alone, cannot be used to indicate organic matter abundance in the core. However, it is useful for determining periods of a euxinic water column. Since Mo/Ti and Ca/Ti are positively correlated, we infer that carbonate cementation is the most important factor in organic matter preservation, which is controlled by the redox state of the water column.

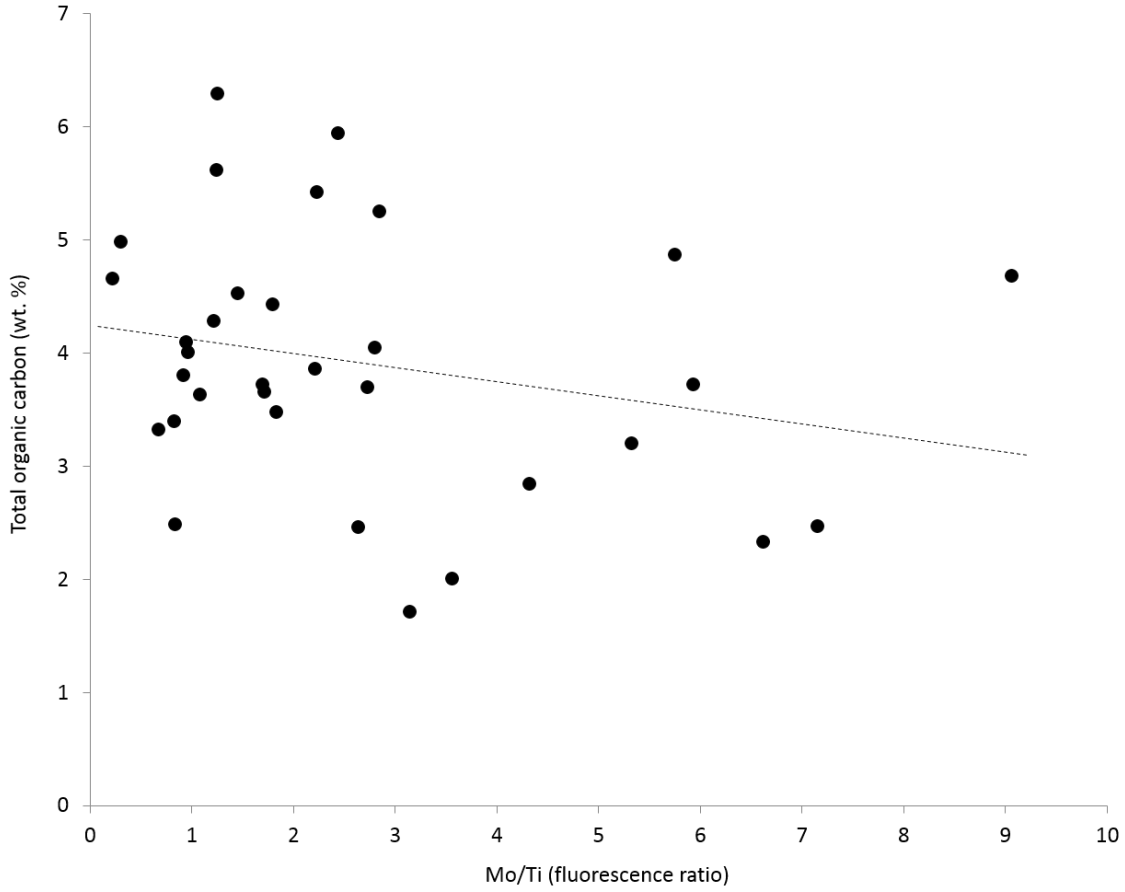

Figure 18. Mo/Ti vs TOC weight percent in the Eagle Ford Group. The regression line has a P-value of 0.18 for a t-test on the regression coefficient.

CONCLUSIONS

Rocks of the Eagle Ford Group deposited under iron-reducing and sulfate-reducing water columns contained significantly more calcium than did rocks deposited under aerobic water columns. This suggests that net carbonate cementation started in the ferruginous zone and continued through the sulfidic zone. The decrease in zone average TOC for the sulfidic zone suggests that carbonate cementation occurred early enough to cause organic matter dilution. Since Mo/Ti fluorescence ratio does not correlate with TOC, it should not be used as an indicator of organic matter, but as an indicator of sulfidic environments.

REFERENCES

Adams, R. L., and J.P. Carr, 2010, Regional depositional systems of the Woodbine, Eagle Ford, and Tuscaloosa of the U.S. Gulf Coast: Gulf Coast Association of Geological Societies Transactions, v. 60, p. 3-27.

Arthur, M., and S. Schlanger, 1979, Cretaceous "Oceanic Anoxic Events" as Causal Factors in Development of Reef-Reservoir Giant Oil Fields: The American Association of Petroleum Geologists Bulletin, v. 63, p. 870-885

Bellanca, A., M. Claps, E. Erba, D. Masetti, R. Neri, I. Premoli Silva, and F. Venezia, 1996, Orbitally induced limestone/marlstone rhythms in the Albian - Cenomanian Cismon section (Venetian region, northern Italy): sedimentology, calcareous and siliceous plankton distribution, elemental and isotope geochemistry: Palaeo, v. 126, p. 227-260.

Bosak, T., and D.K. Newman, 2003, Microbial nucleation of calcium carbonate in the Precambrian: Geology, v. 31, p. 577-580

Breit, G.N., and R.B. Wanty, 1991, Vanadium accumulation in carbonaceous rocks: A review of geochemical controls during deposition and diagenesis: Chemical Geology, v. 91, p. 83-97

Calvert, S.E., and T.F. Pedersen, 1993, Geochemistry of Recent oxic and anoxic marine sediments: Implications for the geological record: Marine Geology, v. 113, p. 67-88

Canfield, D.E., and R. Raiswell, 1991, Carbonate precipitation and dissolution: its relevance to fossil preservation: Taphonomy: Releasing the Data Locked in the Fossil Record, eds. Allison, P.A., Briggs, D.E.G., p. 411-453

Canfield, D.E., and B. Thamdrup, 2009, Towards a consistent classification scheme for geochemical environments, or, why we wish the term 'suboxic' would go away: Geobiology, v. 7, p. 385-392

Charvat, W.A., and R.C. Grayson, Jr., 1981, Anoxic sedimentation in the Eagleford Group (Upper Cretaceous) of Central Texas: Gulf Coast Association of Geological Societies Transactions, v. 31, p. 256

Coleman, M.L., 1985, Geochemistry of diagenetic non-silicate minerals – kinetic considerations: Transactions of the Royal Society of London, A315, p. 39-56

Dawson, W.C., 2006, Shale microfacies: Eagle Ford Group (Cenomanian- Turonian) north-central Texas outcrops and subsurface equivalents: Gulf Coast Association of Geological Societies Transactions, v. 50, p. 607-621

Dawson, W.C., and W.R. Almon, 2010, Eagle Ford Shale Variability: Sedimentologic Influences on Source and Reservoir Character in an Unconventional Resource Unit: Gulf Coast Association of Geological Societies Transactions, v. 60, p. 181-190

Driskell, B., N. Suurmeyer, S. Rilling-Hall, A. Govert, and A. Garbowicz, 2012, Reservoir Description of the Subsurface Eagle Ford Formation, Maverick Basin Area, South Texas, USA: SPE 154528

Fertl, W. H., and H.H. Rieke III, 1979, Gamma ray spectral evaluation techniques identify fractured shale reservoirs and source rock characteristics: SPE: 8454

Froelich, P.N., G.P. Klinkhammer, M.L. Bender, N.A. Luedtke, G.R. Heath, D. Cullen, P. Dauphin, D. Hammond, B. Hartman, and V. Maynard, 1979, Early oxidation of organic matter in pelagic sediments of the eastern equatorial Atlantic: suboxic diagenesis: Geochimica et Cosmochimica Acta, v. 43, p. 1075-1090

Hentz, T.F., and S.C. Ruppel, 2010, Regional lithostratigraphy of the Eagle Ford Shale: Maverick Basin to East Texas Basin: Gulf Coast Association of Geological Societies Transactions, v. 60, p. 325-337

Hildred, G., K. Ratcliffe, and K. Schmidt, 2011, Application of Inorganic Whole-Rock Geochemistry to Shale Resource Plays: an Example from the Eagle Ford Shale, Texas: Houston Geological Society Bulletin, v. 53, p. 31-38

Jenkyns, H.C., 2010, Geochemistry of oceanic anoxic events: Geochemistry, Geophysics, Geosystems, v. 11, p. 1-30

Moredock, D.E., and D.C. Van Siclen, 1964, Regional variation of hydrocarbons in the Edwards Limestone (Cretaceous) of South Texas: Gulf Coast Association of Geological Societies Transactions, v. 14, p. 253-270

Quirein, J., E. Murphy, G. Praznik, J. Witkowsky, S. Shannon, and D. Buller, 2012, A Comparison and Well Log Data to Evaluate Porosity, TOC, and Hydrocarbon Volume in the Eagle Ford Shale: SPE: 159904

Schrag, D. P., J.A. Higgins, F.A. Macdonald, and D.T. Johnston, 2013, Authigenic Carbonate and the History of the Global Carbon Cyle: Science, v. 339, p. 540-543

Scotchman, I.C., 1991, The geochemistry of concretions from the Kimmeridge Clay Formation of southern and eastern England: Sedimentology, v.38, p. 79-106

Sun, Y., and W. Puttmann, 1997, Metal accumulation during and after deposition of the Kupferschiefer from the Sangerhausen Basin, Germany: Applied Geochemistry, v. 12, p. 577-592.

Swindell, G.S., 2012, Eagle Ford Shale – An Early Look at Ultimate Recovery: SPE 158207

Tian, T., W.B. Ayers, and W.D. McCain, 2012, Regional analysis of stratigraphy, reservoir characteristics, and fluid phases in the Eagle Ford Shale, South Texas: Gulf Coast Association of Geological Societies Transactions, v. 62, p. 471-483

Tinnin, B., G. Hildred, and N. Martinez, 2013, Expanding the Application of Chemostratigraphy within the Cretaceous Mudrocks: Estimating Total Organic Carbon and Paleoredox Facies using Major, Minor, and Trace Element Geochemistry: URTeC Annual Meeting, Control ID Number 1579472.

Tissot, F.L.H., N. Dauphas, C.T. Reinhard, T.W. Lyons, D. Asael, and O. Rouxel, 2013, Mo and U Geochemistry and Isotopes: Reading the Archive of Earth's Oxygenation, v. 3, p. 1500-1506

Tribovillard, N., T.J. Algeo, T. Lyons, and A. Riboulleau, 2006, Trace Metals as Paleoredox and Paleoproductivity Proxies: An Update: Chemical Geology, v. 232, p. 12-32.

Van Lith, Y., C. Vasconcelos, R. Warthmann, J.C.F. Martins, and J.A. McKenzie, 2002, Bacterial sulfate reduction and salinity: two controls on dolomite precipitation in Lagoa Vermelha and Brejo do Espinho (Brazil): Hydrobilogia, v. 485, p. 35-49

Visscher, P.T., R.P. Reid, and B.M. Bebout, 2000, Microscale observations of sulfate reduction: correlation of microbial activity with lithified micritic laminae in modern marine stromatolites: Geology, v. 28, p. 919-922

Wanty, R., and M. Goldhaber, 1992, Thermodynamics and kinetics of reactions involving vanadium in natural systems: Accumulation of vanadium in sedimentary rocks: Geochimica et Cosmochimica Acta, v. 56, p. 147-1483.

Warthmann, R., Y. Van Lith, C. Vasconcelos, J.A. McKenzie, and A.M. Karpoff, 2000, Bacterially induced dolomite precipitation in anoxic culture experiments: Geology, v. 28, p. 919-922

Zeng, Z., and M.M. Tice, 2014, Promotion and nucleation of carbonate precipitation during microbial iron reduction: Geobiology, v. 12, p. 362-371